

Light Induced Synaptic Transistor With Dual Operation Modes

Yuanhang Li, Yongchao Yang, Xumin Gao, Jialei Yuan,
Guixia Zhu, Zhiyu Zhang, and Yongjin Wang

Abstract—We propose and fabricate a light induced transistor using a combination of two multiple-quantum-well diodes (MQWDs) with a common n-electrode as the base. Both silicon removal and back wafer etching are conducted to obtain a suspended device architecture. The InGaN/GaN MQWD detects light only when the bias voltage is below the turn-ON voltage and can simultaneously achieve light emission and detection when it turns ON. Therefore, the light induced transistor operates with two distinct light detection modes. The excitatory postsynaptic voltages (EPSVs) are distinct due to the different decay times. Paired-pulse facilitation is experimentally demonstrated to mimic the synaptic plasticity behavior. The EPSV amplitudes are dependent on the pulse interval and pulse number.

Index Terms—InGaN/GaN multiple-quantum-well diode, light induced synaptic transistor, excitatory postsynaptic voltage, paired-pulse facilitation.

I. INTRODUCTION

SYNAPSES receive excitatory stimuli and transmit signals from one neuron to another, which conduct critical computational functions in neural circuits [1]–[3]. In a rat hippocampus, the amplitude of the excitatory postsynaptic currents (EPSCs) is altered by activating the voltage-dependent Ca^{2+} channels when a neurotransmitter is released [4]. A variety of transistors have been demonstrated to artificially emulate biological synapses for the development of synaptic computational systems [5], [6]. On the basis of a conventional CMOS circuit, electronic artificial synapses have been reported with spike-timing dependent plasticity [7]. Carbon nanotube-based synaptic transistors have been proposed for dynamic logic and learning using mobile protons [8], [9]. Ion migration has been adopted for use in electrolyte-gated transistors [8]. Energy-efficient and solution-processed flexible IGZO electric-double-layer transistors are fabricated to mimic synaptic behaviors [10]–[12].

Here, we propose and fabricate a suspended light induced transistor that consists of two InGaN/GaN multiple-quantum-

Manuscript received August 30, 2016; revised September 8, 2016; accepted September 8, 2016. Date of publication September 9, 2016; date of current version October 21, 2016. This work was supported in part by the National Natural Science Foundation of China under Grant 61322112 and Grant 61531166004, and in part by the Research Projects 2014CB360507, RLD201204, and BJ211026. The review of this letter was arranged by Editor S.-J. Chang.

Y. Li, Y. Yang, X. Gao, J. Yuan, G. Zhu, and Y. Wang are with the Grünberg Research Centre, Nanjing University of Posts and Telecommunications, Nanjing 210003, China (e-mail: wangyj@njupt.edu.cn).

Z. Zhang is with the Changchun Institute of Optics, Fine Mechanics and Physics, Chinese Academy of Sciences, Changchun 130033, China.

Color versions of one or more of the figures in this letter are available online at <http://ieeexplore.ieee.org>.

Digital Object Identifier 10.1109/LED.2016.2607998

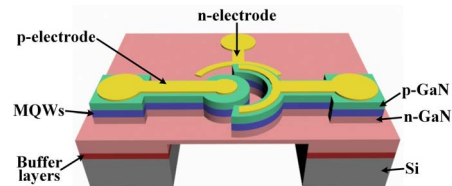


Fig. 1. Schematic cross section of the integrated devices.

well diodes (MQWDs) with a common n-contact as the base, as shown in Fig. 1. The collector detects light generated from the emitter to complete the photon-to-electron conversion [13]. As an InGaN/GaN MQWD, the collector simultaneously exhibits light detection ability when it emits light, resulting in dual operation modes for the light induced transistor. The proposed light induced transistor demonstrates an excitatory postsynaptic voltage (EPSV) and paired-pulse facilitation behavior, which are analogous to that in biological synapse. Such light induced synaptic transistors are promising for building neural circuits using photons.

II. EXPERIMENTAL RESULTS AND DISCUSSIONS

The suspended light induced synaptic transistor was implemented on a 2-inch GaN-on-silicon wafer with p-n junction InGaN/GaN multiple-quantum-well structures [14]. The top device layers consist of an 80-nm-thick p-GaN layer, a 35-nm-thick p-AlGaN layer, a 120-nm-thick InGaN/GaN MQWs layer, a 3400-nm-thick n-GaN layer, a 400-nm-thick undoped GaN layer, a 600-nm-thick AlGaN buffer layer and a 330-nm-thick AlN layer. Both the mesa and separation trench were initially defined on the top using photolithography. Inductively coupled plasma reactive ion etching was conducted, and the top device layer was etched down to the n-GaN layer. The Cl_2 and BCl_3 hybrid gases were used at the flow rates of 10 sccm and 25 sccm, respectively. The 1.6- μm -thick AZ5214 photoresist served as the etching hard mask. Subsequently, both p- and n-type electrodes were formed using a lift-off technique after evaporating the 20 nm Ni/180 nm Au bilayers. The device was then annealed at 500°C in a N_2 atmosphere for 5 min to obtain p- and n-contacts. The bottom etching window was patterned using backside alignment photolithography, and then silicon removal and back wafer thinning were performed to obtain a membrane-type light induced synaptic transistor, which was finally generated on a ~2- μm -thick suspended membrane by removing the residual photoresist.

GaN is with excellent mechanical properties to support suspended device structure [15], which can form highly-confined waveguide architecture due to the large index contrast between

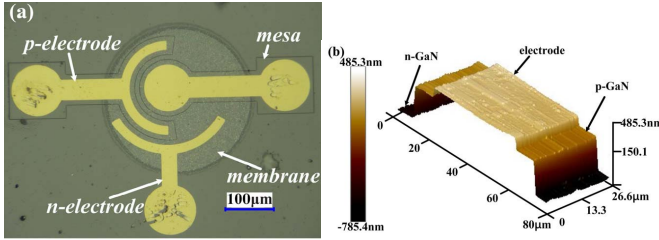


Fig. 2. (a) Optical micrograph of light induced synaptic transistor; (b) atomic force microscope image of suspended device.

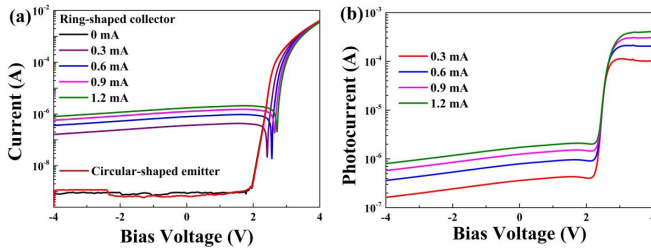


Fig. 3. (a) Log-scaled I-V plots for the ring-shaped collector versus the injection currents of the circular-shaped emitter; (b) normalized photocurrent.

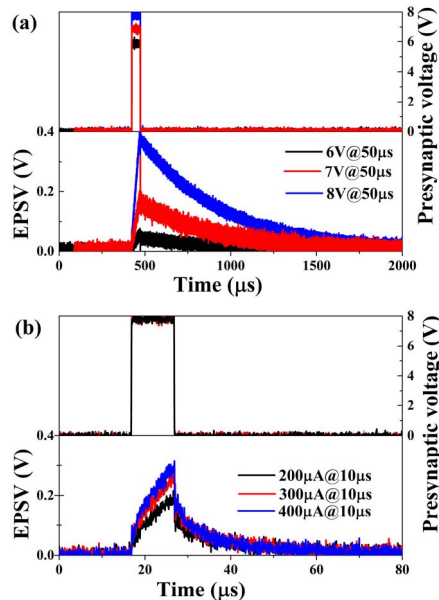


Fig. 4. (a) Measured EPSV under light detection mode; (b) EPSV triggered by pulses under light emission and detection modes.

air and GaN. Figure 2(a) shows one optical micrograph of a suspended light induced synaptic transistor. The n-electrode was used as the common base, and the two InGaN/GaN MQWDs were adopted as either the emitter or the collector, creating a light induced transistor. Except for the square contact pads, the p-electrode and n-electrode were fabricated on a suspended membrane of 300 μm in diameter. A 10-μm-wide isolation trench was used to separate the ring-shaped and circular-shaped p-electrode parts. Figure 2(b) illustrates a three-dimensional atomic force microscope image of the suspended mesas. The measured mesa height was 620 nm, and the Ni/Au bilayers were 200 nm thick.

As the ring-shaped InGaN/GaN MQWD was adopted as

the collector and the circular-shaped MQWD was adopted as the emitter, the collector absorbed the light generated from the emitter to achieve the photon-to-electron conversion, giving rise to an induced photocurrent. Three-terminal measurements were taken from the light induced transistor using an Agilent B1500A semiconductor device analyzer. Figure 3(a) shows the log-scaled current-voltage (I-V) plots. Both the ring-shaped MQWD and the circular-shaped MQWD exhibit the similar rectifying behaviors. The measured current was the induced photocurrent caused by the light emission for the circular-shaped MQWD when the bias voltage was lower than the turn-on voltage. Many more photons were generated when the injection current of the emitter increased from 0 mA to 1.2 mA. Therefore, the collector absorbed more light, and the induced electron-hole pairs were increased, leading to an improved photocurrent. In this light detection mode, the MQWD serves as simply a photodiode to sense the light. In principle, the InGaN/GaN MQWD can detect and emit light at the same time when the MQWD is turned on. The measured current is the sum of the driven current and the induced photocurrent during this operation mode. The current values of the ring-shaped collector that was measured at the injection current of 0 mA for the circular-shaped emitter subtracted the measured current values at the various injection currents to obtain the normalized photocurrent. The barrier of the collector was managed and thus the absorbed light could generate much more electron-hole pairs when the collector operated under the latter mode, leading to a significantly enhanced photocurrent, as illustrated in Fig. 3(b). Except for detecting in-plane light, the membrane-type device architecture enables the transistor to sense the out-of-plane incident light from either the top or bottom interface.

The pulse performance of the light induced transistor was characterized. As a light induced synaptic transistor, the excitatory postsynaptic voltage (EPSP) was clearly observed at the ring-shaped collector when a pulse signal was applied to the circular-shaped emitter, as illustrated in Fig. 4(a). The driving current of the collector was 0 mA. The excited signals exhibited clear decay behaviors after the pulsed signal excitation and gradually returned back towards their initial states. Both the decay time and the amplitude of the pulse signal were increased with increasing the pulse voltage from 6 V to 8 V. When the collector was driven, the collector emitted and detected light at the same time. The pulse signals were applied to the emitter and the measured EPSPs were shown in Fig. 4(b). The decay time was different and greatly decreased, which was inconsistent with the measured photocurrent. With increasing the driven current, the EPSP amplitude was increased.

When two pulse signals were applied in short succession to the circular-shaped emitter, the amplitude of the second EPSP at the collector was larger than the first. This process is known as paired-pulse facilitation (PPF). Figure 5(a) shows the measured EPSPs at the ring-shaped collector triggered by a pair of pulse signals (50 μs, 7 V), in which the driven current is 0 mA, and the pulse interval, Δt , is 1 μs. The amplitude of the second EPSP was inversely related to the amplitude of the first, and PPF behavior occurred because

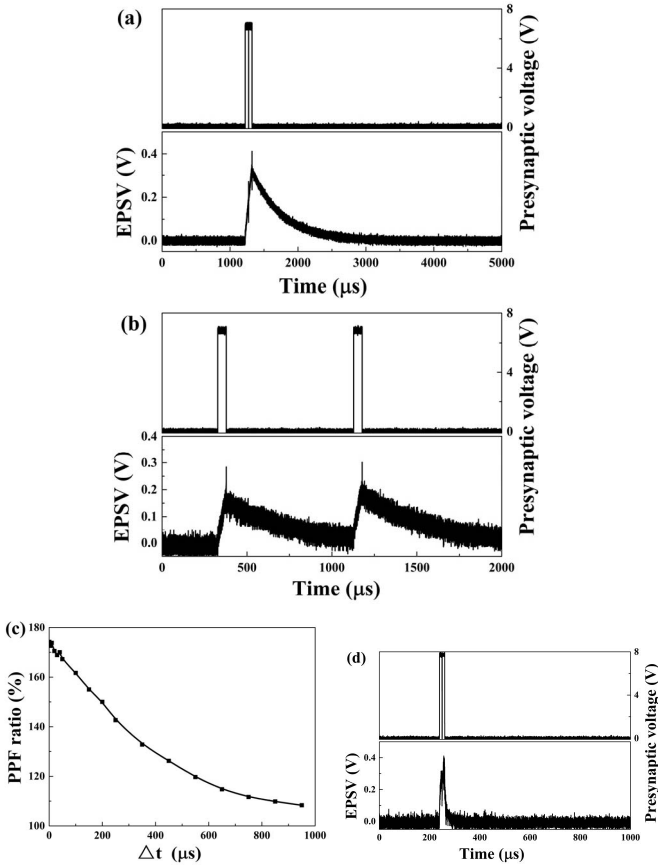


Fig. 5. (a) PPF with a pulse interval of $1\ \mu\text{s}$; (b) PPF behavior with a pulse interval of $750\ \mu\text{s}$; (c) PPF ratio as a function of the pulse interval; (d) PPF behavior under light emission and detection modes.

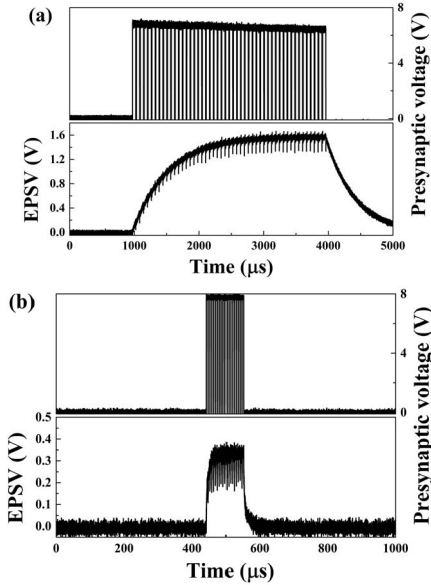


Fig. 6. (a) Pulse number-dependent EPSV under light detection mode; (b) pulse number-dependent EPSV under light emission and detection modes.

the $1\ \mu\text{s}$ pulse interval was shorter than the decay time. The second response is superimposed on the first. The amplitude of the second EPSV was approximately 1.7 times that of the first EPSV triggered by the first pulsed signal. As the pulse interval grew larger than the decay time, the second EPSV was normally independent of the first EPSV, as shown in Fig. 5(b)

with a pulse interval, Δt , of $750\ \mu\text{s}$. Figure 5(c) illustrates the PPF ratio ($\text{EPSV}_2/\text{EPSV}_1$) as a function of the pulse interval. The pulse interval-dependent PPF decay characteristic was clearly observed. On the other hand, the collector operated under emission and detection mode when the driven current was $0.6\ \text{mA}$. Figure 5(d) shows the measured EPSVs triggered by a pair of pulse signals ($10\ \mu\text{s}, 8\ \text{V}$), separated by a pulse interval, Δt , of $1\ \mu\text{s}$. The amplitude of the second response was larger than the first, meaning that PPF behavior occurred under this operation mode. Correspondingly, the second EPSV rapidly became independent of the first EPSV because the decay time was shorter.

To investigate the pulse facilitation behavior further, Figure 6(a) shows the pulse number-dependent EPSV. The pulse number was 100 with a fixed pulse interval of $10\ \mu\text{s}$, and the collector operated under detection mode. The EPSV amplitude increased and eventually was saturated as the pulse number grew. The measured 100th EPSV amplitude was approximately 6.4 times the first. Figure 6(b) illustrates the measured EPSV under simultaneous emission and detection mode. The applied pulse was ($5\ \mu\text{s}, 8\ \text{V}$), and the pulse number was 20 with a fixed pulse interval of $0.5\ \mu\text{s}$. Similar pulse number-dependent EPSV performance was also observed.

III. CONCLUSION

In summary, light induced transistors were fabricated using a combination of two InGaN/GaN MQWDs with a common n-electrode as the base. Both silicon removal and back wafer etching were conducted to obtain suspended device architecture. The light induced transistor exhibited two distinct light detection modes. One was that the collector only detects light, and the other was that the collector simultaneously emits and detects light. PPF was experimentally demonstrated to mimic synaptic plasticity behavior. The EPSV amplitudes were dependent on the pulse interval and the pulse number.

REFERENCES

- [1] S. Song, K. D. Miller, and L. F. Abbott, "Competitive Hebbian learning through spike-timing-dependent synaptic plasticity," *Nature Neurosci.*, vol. 3, no. 9, pp. 919–926, 2000.
- [2] L. F. Abbott and W. G. Regehr, "Synaptic computation," *Nature*, vol. 431, pp. 796–803, Oct. 2004. doi: 10.1038/nature03010.
- [3] V. M. Ho, J.-A. Lee, and K. C. Martin, "The cell biology of synaptic plasticity," *Sci.*, vol. 334, pp. 623–628, no. 6056, Nov. 2011, doi: 10.1126/science.1209236.
- [4] D. Debanne, N. C. Guérineau, B. H. Gähwiler, and S. T. Thompson, "Paired-pulse facilitation and depression at unitary synapses in rat hippocampus: Quantal fluctuation affects subsequent release," *J. Physiol.*, vol. 491, no. 1, pp. 163–176, Feb. 1996, doi: 10.1113/jphysiol.1996.sp021204.
- [5] L. Q. Zhu, C. J. Wan, L. Q. Guo, Y. Shi, and Q. Wan, "Artificial synapse network on inorganic proton conductor for neuromorphic systems," *Nature Commun.*, vol. 5, pp. 1–7, Jan. 2014, doi: 10.1038/ncomms4158.
- [6] C. J. Wan, L. Q. Zhu, Y. H. Liu, P. Feng, Z. P. Liu, H. L. Cao, P. Xiao, Y. Shi, and Q. Wan, "Proton-conducting graphene oxide-coupled neuron transistors for brain-inspired cognitive systems," *Adv. Mater.*, vol. 28, no. 18, pp. 3557–3563, May 2016, doi: 10.1002/adma.201505898.
- [7] G. Indiveri, E. Chicca, and R. Douglas, "A VLSI array of low-power spiking neurons and bistable synapses with spike-timing dependent plasticity," *IEEE Trans. Neural Netw.*, vol. 17, no. 1, pp. 211–221, Jan. 2006.
- [8] K. Kim, C.-L. Chen, Q. Truong, A. M. Shen, and Y. Chen, "A carbon nanotube synapse with dynamic logic and learning," *Adv. Mater.*, vol. 25, no. 12, pp. 1693–1698, Mar. 2013, doi: 10.1002/adma.201203116.

- [9] A. M. Shen, C.-L. Chen, K. Kim, B. Cho, A. Tudor, and Y. Chen, "Analog neuromorphic module based on carbon nanotube synapses," *ACS Nano*, vol. 7, no. 7, pp. 6117–6122, Jun. 2013, doi: 10.1021/nn401946s.
- [10] J. Zhou, C. Wan, L. Zhu, Y. Shi, and Q. Wan, "Synaptic behaviors mimicked in flexible oxide-based transistors on plastic substrates," *IEEE Electron Device Lett.*, vol. 34, no. 11, pp. 1433–1435, Nov. 2013, doi: 10.1109/led.2013.2280663.
- [11] J. M. Zhou, N. Liu, L. Q. Zhu, Y. Shi, and Q. Wan, "Energy-efficient artificial synapses based on flexible IGZO electric-double-layer transistors," *IEEE Electron Device Lett.*, vol. 36, no. 2, pp. 198–200, Feb. 2015, doi: 10.1109/LED.2014.2381631.
- [12] X. Wan, Y. Yang, P. Feng, Y. Shi, and Q. Wan, "Short-term plasticity and synaptic filtering emulated in electrolyte-gated IGZO transistors," *IEEE Electron Device Lett.*, vol. 37, no. 3, pp. 299–302, Mar. 2016, doi: 10.1109/LED.2016.2517080.
- [13] W. Cai, X. M. Gao, W. Yuan, Y. C. Yang, J. L. Yuan, H. B. Zhu, and Y. J. Wang, "Integrated p-n junction InGaN/GaN multiple-quantum-well devices with diverse functionalities," *Appl. Phys. Exp.*, vol. 9, no. 5, p. 052204, 2016, doi: 10.7567/APEX.9.052204.
- [14] Y. J. Wang, G. X. Zhu, W. Cai, X. M. Gao, Y. C. Yang, J. L. Yuan, Z. Shi, and H. B. Zhu, "On-chip photonic system using suspended p-n junction InGaN/GaN multiple quantum wells device and multiple waveguides," *Appl. Phys. Lett.*, vol. 108, no. 16, p. 162102, 2016, doi: 10.1063/1.4947280.
- [15] Y. J. Wang, T. Sasaki, T. Wu, F. R. Hu, and K. Hane, "Comb-drive GaN micro-mirror on a GaN-on-silicon platform," *J. Micromech. Microeng.*, vol. 21, no. 3, p. 035012, 2011, doi: 10.1088/0960-1317/21/3/035012.